Improved imaging and preservation of lysosome dynamics using silver nanoparticle-enhanced fluorescence

Sumaiya A. Soha[1,2], Araniy Santhireswaran[2], Gregory K. Hodgson[2], Michael Sugiyama[2], Costin N. Antonescu[1,2*], Stefania Impellizzeri[1,2*], Roberto J. Botelho[1,2*]

[1]Molecular Science Graduate Program and [2]Department of Chemistry and Biology, Ryerson University, Toronto, Ontario, Canada, M5B 2K3

*Correspondence should be sent to:

Dr. Costin N. Antonescu at cantonescu@ryerson.ca

Dr. Stefania Impellizzeri at simpellizzeri@ryerson.ca

Dr. Roberto J. Botelho at rbotelho@ryerson.ca

Lead author: Dr. Roberto J. Botelho

Running title: Metal-enhanced fluorescence in cells

Keywords

Fluorescence, live-cell microscopy, surface plasmons, lysosomes, macrophages, nanomaterials, inter-disciplinary, phototoxicity

Summary

The dynamics of living cells can be studied by live-cell fluorescence microscopy. However, this often requires the use of excessive light energy to obtain good signal-to-noise ratio, which can then photobleach the fluorochromes used, and more worrisome, lead to photo-toxicity. Thus, strategies that can reduce the amount and/or exposure to excitation light would improve live-cell microscopy. Upon light excitation, noble metal nanoparticles such as silver (AgNP) generate plasmons, which can amplify the excitation of fluorophores that are proximal to the surface of the nanoparticle. These can also couple to the oscillating dipole of nearby radiating fluorophores, which modifies the rate of emission and enhances their fluorescence. Here, we show that AgNP fed to cells to accumulate within lysosomes enhanced the fluorescence of lysosome-targeted BODIPY-cholesterol and DQ-BSA. Moreover, AgNP increased the fluorescence of GFP fused to the cytosolic tail of LAMP1, showing that metal enhanced fluorescence occurs across the lysosomal membrane. Importantly, by using AgNP, we could track lysosome motility with reduced laser power without damaging and altering lysosome dynamics. Overall, AgNP-enhanced fluorescence may be a useful tool to study the dynamics of the endo-lysosomal pathway while minimizing photo-toxicity.

Introduction

Live-cell fluorescence microscopy is an essential tool to determine and characterize the spatio-temporal dynamics of molecules, supra-molecular assemblies, organelles, and of entire cells (Jensen, 2013; Lidke and Lidke, 2012). Over the years, technological enhancements have emerged that pushed the boundary in the spatial resolution of cellular organization, the detection limits of cameras and photo-detectors allowing for single-molecule imaging, and image analysis that permits high-throughput, high-content and unbiased quantification (Boutros et al., 2015; Jing et al., 2021; Lidke and Lidke, 2012; Shashkova and Leake, 2017). These improvements depended and continue to depend on innovative manipulation of the physico-chemical properties of fluorochromes, hardware advances leading to superior camera sensitivity and detection, and a surge in computational power and better algorithms (Boutros et al., 2015; Lidke and Lidke, 2012; Moen et al., 2019; Ouyang et al., 2018; Peterson et al., 2016; Rust et al., 2006; Shtengel et al., 2009). Yet, challenges related to photo-bleaching and photo-toxicity remain when observing living samples by fluorescence microscopy, which lead to loss of signal, and more troublesome, artifactual observations (Boudreau et al., 2016; Icha et al., 2017; Tinevez et al., 2012). These issues are most often caused by excessive light energy used during excitation, particularly blue light, which generates reactive oxygen species (ROS) that ultimately destroy fluorochromes and impair cell function (Boudreau et al., 2016; Icha et al., 2017; Tinevez et al., 2012; Waldchen et al., 2015). Thus, the need remains to develop brighter and more stable fluorochromes, more sensitive detection tools, and/or elegant manipulation of the physico-chemical properties of light and materials to further offset photo-bleaching and photo-damage.

Surface plasmons of noble metal nanoparticles are a promising means to enhance the emission intensity of fluorescent probes without the need to synthetically alter their chemical

structure (Bouhelier et al., 2004; Ekgasit et al., 2004b, 2004a; Hodgson et al., 2020; Lakowicz et al., 2003; Peterson et al., 2016; Petryayeva and Krull, 2011). Plasmon excitation can be described as the collective oscillation of conduction band electrons on the surface of metal nanostructures following the incidence of a photon of appropriate wavelength (Barnes et al., 2003; Hao and Schatz, 2004; Liz-Marzán, 2006; Moores and Goettmann, 2006; Odom and Schatz, 2011). This effect translates into the enhancement of the electromagnetic field in proximity to the surface of the nanoparticles.

Silver nanoparticles (AgNP) are capable of interacting with light along the visible and near-infrared regions of the electromagnetic spectrum, and can significantly affect the photophysical processes underlying the emission of fluorescent molecules up to 200 nm, depending on the overlap of fluorophores' emission spectra with the scattering component/s of the nanoparticles' extinction spectra (Anger et al., 2006; Aslan et al., 2005; Fu et al., 2007; Fu and Lakowicz, 2007; Lakowicz, 2005; Lakowicz et al., 2008, 2003, 2002). This phenomenon is generally described as metal-enhanced fluorescence (MEF) and arises from near-field interactions between AgNP and a fluorochrome. This interaction ultimately enhances fluorescence by increasing the rate of fluorophore excitation (i.e., the enhanced electromagnetic field resulting from plasmonic excitation of AgNP increases the probability of excitation) and/or by increasing the radiative decay rate, which is proportional to the quantum yield of fluorescence (Hodgson et al., 2020). The latter mechanism occurs by coupling between the plasmon resonance oscillation of AgNP and the oscillating dipole of radiating fluorophores, effectively forming a radiative AgNP-fluorophore complex, often referred to as a "plasmophore". Relative to the fluorochrome alone, the plasmophore exhibits a much lower excited state lifetime and a higher radiative decay rate, resulting in a higher quantum yield of emission (Lakowicz et al., 2008). Both components of MEF

– increased excitation and increased quantum yield – ultimately contribute to enhanced brightness. Moreover, MEF can also improve photostability and reduce blinking (Fu and Lakowicz, 2007; Malicka et al., 2003).

Due to these reasons, the application of MEF by AgNP has considerable potential to improve fluorescence imaging of biological components. Due to the membrane impermeability of AgNP, MEF is best geared to enhance fluorescence of fluorochromes *in vitro*, or positioned on the cell surface, or within the endo-lysosomal compartments after pinocytosis. The endocytic pathway captures and processes extracellular and membrane-bound cargo and receptors for recycling or targeting to lysosomes (Huotari and Helenius, 2011; Naslavsky and Caplan, 2018; Norris and Grant, 2020). Therefore, AgNP are likely to be internalized by pinocytosis and trafficked to lysosomes. Lysosomes are a heterogeneous collection of acidic organelles that host numerous degradative enzymes, and are thus responsible for degrading internalized macromolecules, autophagic material, and particles engulfed by phagocytosis (Inpanathan and Botelho, 2019; Kiselyov et al.; Luzio et al., 2007; Saffi and Botelho, 2019). Depending on the cell type, there are 100-1000 lysosomes per cell; these organelles are highly dynamic and can differ in their subcellular distribution, their motility, and fusion-fission cycling. These fusion and fission events can be at the whole-organelle level or may occur through tubular intermediates that aid in exchange of cargo (Balderhaar and Ungermann, 2013; Bissig et al., 2017; Bright et al., 2005; Choy et al., 2018).

Importantly, the labeling or illumination conditions typically required for fluorescence microscopy imaging have been shown to damage the endo-lysosomal system. For example, staining with acridine orange or Lysotracker, both used to detect acidic pH of lysosomes, can cause lysosome rupture when combined with light (Pierzyńska-Mach et al., 2014). Similarly, endo-

lysosomal dynamics in macrophages was altered during live-cell spinning disc confocal imaging (Choy et al., 2018; Saffi et al., 2021). In part, this is mediated by reactive oxygen species formed during imaging, which can alter microtubule and actin dynamics (Choy et al., 2018; Saffi et al., 2021). In turn, altered microtubule and actin dynamics can disrupt lysosome fusion-fission cycles and transport (Bissig et al., 2017; Bright et al., 2005; Hong et al., 2015; Johansson et al., 2007; Keren-Kaplan et al., 2022; Kumar et al., 2022; Saffi et al., 2021). Fluorescence methods that reduce excitation energy and/or increase emission signal could reduce artifacts when investigating the endo-lysosomal system (Choy et al., 2018; Saffi et al., 2021).

Here, we postulated that AgNP would accumulate in lysosomes and could be used to enhance fluorescence of lysosome-targeted probes. In fact, we observed that AgNP enhanced the fluorescence of boron dipyrromethene (BODIPY) dyes *in vitro* and within lysosomes after delivery of BODIPY-labelled cholesterol or the dye-quenched DQ-BSA, which is used to measure protein degradation, and boosted the fluorescence of GFP fused to the cytosolic tail of LAMP1, a lysosomal membrane protein. As a result, we were able to reduce the excitation energy while obtaining good signal-to-noise ratio, allowing dynamic studies of lysosomes by preserving lysosome motility. We propose that AgNP loading into lysosomes may be useful to study lysosome dynamics while mitigating photo-bleaching and photo-toxicity.

Materials and Methods

Synthesis of silver nanoparticles

Chemicals were purchased from Sigma-Aldrich and Fisher Scientific. To a clean, oven-dried 50 mL Erlenmeyer flask, 34.4 mL of MilliΩ H_2O (Millipore Purification System), 4.0 mL of 10 mM trisodium citrate, 0.80 mL of 10 mM of 2-Hydroxy-4′-(2-hydroxyethoxy)-2-methylpropiophenone

(Irgacure®-2959, I-2959) and 0.8 mL of 10 mM $AgNO_3$ solutions were added. The mixture was degassed with N_2 for 30 min, after which it was irradiated at 365 nm for 10 min in a Luzchem LCZ-4 photoreactor (14 bulbs, 100 W/m^2) to yield a dark yellow solution of AgNP which was used as prepared. The obtained AgNP are ~3 nm in diameter and are stable in solution up to 6 months (Stamplecoskie and Scaiano, 2012, 2010).

Spectroscopy

Steady-state absorption spectra were recorded with an Agilent Cary 60 UV-visible spectrophotometer, using quartz cells with a path length of 1 cm. Steady-state emission and synchronous scattering spectra were recorded with an Agilent Cary Eclipse spectrofluorimeter in aerated solutions.

AgNP casting and dye-embedded gelatin films

About 50-250 µL of AgNP suspension was dropcasted onto a clean, sterile 20x20 mm coverslip and dried overnight in the dark. We then prepared and filter-sterilized 0.2% (v/v) gelatin solution in ddH_2O and added to a final concentration of 200 µM BODIPY™ 493/503 (4,4-Difluoro-1,3,5,7,8-Pentamethyl-4-Bora-3a,4a-Diaza-s-Indacene; ThermoFisher) or 10 µg/mL BODIPY-cholesterol (ThermoFisher). We then added dropwise 150 µL of the BODIPY or BODIPY-cholesterol gelatin mixture onto coverslips previously coated with AgNP and incubated in the dark at room temperature for 5 min to solidify the gelatin. The coverslip was then lifted to pool the excess liquid at a corner and excess solution was aspirated by vacuum, leaving a thin film on the coverslip. The coverslips were left for an additional 20 min for the gelatin film to dry completely before imaging.

Cell culture, plasmids, and transfection

The male-mouse macrophage-like RAW 264.7 cell line was obtained from ATCC (TIB-71, VA, USA) and cultured in DMEM with 5% heat inactivated fetal bovine serum, re-seeded every 2-3 days. The Cos7 cell line is a kidney fibroblast-like cell derived from a male-green monkey and was obtained from ATCC (CRL-1651) and were cultured in DMEM with 10% fetal bovine serum. Both cell types were plated at 30-50% confluency and used within 24-48 h. Plasmid encoding LAMP1-GFP was obtained from Addgene (Plasmid #34831) and previously characterized by (Falcón-Pérez et al., 2005). Transfection was done with FuGENE (Promega, Madison, WI) as recommended by the manufacturer and cells were observed within 24 h.

Pinocytosis of AgNP and lysosomal dyes

RAW and Cos7 cells were seeded at 70% confluency the day prior to imaging. Cells were then washed 1x with PBS and immersed with fresh 2 mL DMEM media supplemented with 5% FBS to which 50 or 250 µL of AgNP suspension was added. Cells were then incubated at 37 °C for 1 h in the dark to permit internalization of AgNP suspension. After this, cells were washed 1x with PBS and immediately replenished with 1 mL of DMEM. Cells were then incubated with 10 µg/mL DQ-BSA (ThermoFisher, Burlington, ON) for 1 h, then washed in PBS and imaged in DMEM medium free of phenol red. Alternatively, cells were labelled with 10 µg/mL BODIPY-cholesterol for 40 min, then washed in PBS and imaged in DMEM medium free of phenol red.

Live-cell spinning disc confocal microscopy

Cells were imaged by live-cell spinning disc confocal microscopy using a Quorum DisKovery Spinning Disc Confocal microscope system equipped with a Leica DMi8 microscope connected to a iXon Ultra 897 EMCCD BV camera and controlled by Quorum WaveFX powered by MetaMorph software (Quorum Technologies, Guelph, ON). Imaging was done with a 63x oil immersion objective and 100 µm pinhole disc. Imaging settings during each session were kept the same with typical settings as follows: electron-multiplying gain of 50, exposure of 100 ms, and the laser power set to 50 mW. Lower laser light exposure was used at 10 ms exposure, 10 mW laser power, and an electron-multiplying gain of 50. Single plane images were acquired with the brightfield channels and appropriate laser and filter settings. Images were 16-bit and 512 x 512.

Incucyte imaging and quantification of confluency and CellTox Green staining

RAW macrophages were seeded into a 6-well plate at 30-50% confluency. The next day, cells were labelled with vehicle, 50 µL of AgNPs, or 250 µL of AgNPs as before, followed by 1 µL/mL CellTox Green (Promega). Alternatively, cells were treated with 5 µM staurosporine (Abcam, Cambridge, MA) and CellTox Green as a positive control for cell death. Immediately after adding the treatments and CellTox Green, cells were imaged using the Incucyte SX5 Live-Cell Analysis Instrument (Sartorius, Gottingen, Germany). Cells were imaged using the phase and green channels for 24 h every 30 min, using the 10x objective lens. Images were analysed at each frame by calculating the percent area covered by cells (phase imaging) and the number of CellTox Green-labelled cells using particle detection module after thresholding and subtracting background fluorescence.

Image analysis and quantification

Image analysis was performed with FIJI. The fluorescence intensity of 16-bit images or regions of interest (single cells) was measured by subtracting background. Due to variation between experiments in the absolute values in fluorescence, means were normalized as indicated. For visualization, images were window balanced with conditions that yielded highest intensity and propagated to other open images without altering pixel values. The number of images or cells quantified per condition and per experiment are indicated in the relevant figure legends.

Particle tracking and lysosome motility

Lysosome motility was quantified using TrackMate plug-in for ImageJ/FIJI (NIH, Bethesda, MD). Briefly, individual cells were selected and subject to TrackMate analysis (Tinevez et al., 2017). Particle size was set to 10 pixels across all conditions, while thresholding was modified to track 5-10 puncta per cell, eliminating noise. The Simple LAP Tracker was selected and the linking max distance, gap-closing max distance, and gap closing max frame gap were maintained at the default values of 15, 15, and 2, respectively. No additional filters were applied to avoid bias. Velocity analysis was extracted and used to quantify lysosome motility.

Statistical analysis

Experiments were repeated a minimum of three independent times or as indicated. For single-cell analysis, 15-50 cells were quantified per experiment per condition as indicated in figure legends. Unless otherwise indicated, means or normalized means and the associated standard error of the mean (SEM) of the independent experiments were calculated and statistically analysed. Unless otherwise stated, data was assumed to be normally distributed, Student's t-test was used to compare experiments with two conditions, and one-way ANOVA and post-hoc test like Tukey's

test was used to test the mean between three or more conditions. Statistical analysis and data presentation was done with GraphPad Prism version 9.

Results

AgNP enhances BODIPY fluorescence in vitro

To assess the ability of AgNP to enhance fluorescence, we synthesized small AgNP (Ag "seeds") averaging 3 nm in diameter through a photochemical method. Upon ultraviolet (365 nm) illumination, the free radical initiator I-2959 can undergo a Norrish II cleavage to produce ketyl radicals (Fig. 1A). To maximize the photochemical cleavage of I-2959, as well as minimizing quenching of the photoproducts by oxygen, the solutions were purged with N_2 for 30 min prior to irradiation. The photogenerated ketyl radicals can then reduce Ag^+ to Ag^0, leading to the formation of AgNP.

The extinction spectrum of AgNP (Fig. 1B, black trace) shows the absorption of the plasmon resonance band at 390 nm, while the nanoparticles are not fluorescent. We then sought to determine if these AgNP could enhance the fluorescence of model fluorochromes. For this purpose, we selected BODIPY, which displays maxima of absorption at ~ 490 nm and emission at ~ 520 nm (Fig. 1B, green traces). Previously, we demonstrated that the fluorescence of green-emitting probes based on the BODIPY platform can experience MEF by large triangular silver nanoplates (~ 80 nm), for which the surface plasmon band is centred at 660 nm (Dogantzis et al., 2020; Golian et al., 2021; Hodgson et al., 2020). Indeed, large, non-spherical nanoparticles are known to exhibit increased scattering (Knoblauch et al., 2020; Lakowicz, 2005; Lakowicz et al., 2008). Nevertheless, while it is true that the scattering component of the extinction spectrum of

AgNP tends to be greater for larger nanostructures of the same shape, it is the overlap between the emission spectrum of the dye and the nanoparticle scattering that is essential for MEF. In our case, the synchronous scattering ($\lambda_{Ex} = \lambda_{Em}$) spectrum of AgNP (Dragan et al., 2013; Hodgson et al., 2020; Knoblauch et al., 2020) shows that the scattering component of the AgNP extinction well overlaps with the emission of BODIPY (Fig. S1, Supplementary Information).

In parallel, spectral overlap between the emission of the fluorophore and the absorption component of the nanoparticle's extinction would be expected to quench fluorescence through the formation of non-radiative plasmophores. As shown in Fig. 1B however, minimal overlap exists between the fluorescence emission of BODIPY and the intrinsic absorption (where the synchronous scattering decreases) of AgNP in this system. It is worth noting here that the underlying requirement for MEF is ultimately the activation of surface plasmons, which can indeed be achieved by the emission of nearby fluorophores, or by the same far-field irradiation used to excite the organic dye (in this work, λ_{Ex} = ~488 nm). Although the extinction of AgNP at 488 nm is weak (Fig. 1B), we do not exclude a synergistic contribution of direct plasmon resonance excitation.

Next, we embedded BODIPY in a gelatin film, placing this onto a coat of AgNP dry casted onto a coverslip to determine if AgNP boosted the fluorescence of BODIPY fluorochromes *in vitro*. In this setup, the AgNP coating on the coverslips forms a separate layer onto which the BODIPY-containing gelatin film is formed, allowing MEF to occur in a spatially-defined manner. First, we observed that gelatin films encasing the BODIPY dye and placed onto a coverslip without AgNP emitted low and diffused fluorescence by confocal imaging, but which was higher than coverslips containing only AgNP without fluorophore (Fig. 2A, 2B). However, in the presence of AgNP, bright spots were observed of different sizes and morphologies (Fig. 2A, 2B). Overall, the

total fluorescence intensity of the image fields containing both BODIPY and AgNP was significantly higher (~4x) than with BODIPY-alone, while both were higher than AgNP alone (Fig. 2B). To complement this experiment, we also used a similar strategy for BODIPY-cholesterol embedded in gelatin films placed on coverslips coated with AgNP and compared these to BODIPY-cholesterol gelatin films on uncoated coverslips. We observed that BODIPY-cholesterol alone formed fluorescence puncta, possibly corresponding to cholesterol aggregates (Fig. 2C). This condition produced higher fluorescence than AgNP alone (Fig. 2D). However, relative to BODIPY-cholesterol alone, the fluorescence intensity of gelatin-fields containing BODIPY-cholesterol and placed on coverslips coated with AgNP was again significantly higher at ~3-fold increase (Fig. 2D). Overall, these data suggest that AgNP enhance the fluorescence of free or conjugated BODIPY *in vitro*.

AgNP are non-toxic to macrophages

We then tested if macrophages allowed to pinocytose AgNP would display signs of cytotoxicity before determining if AgNP could enhance fluorescence intracellularly. We used RAW macrophages as our primary cell model because of their proficiency for fluid phase endocytosis and trafficking to lysosomes. To test for cytotoxicity, we allowed cells to pinocytose 50 µL or 250 µL of AgNP suspension for 24 h, estimating 1.261×10^{11} particles per µL of AgNP suspension (see Supplementary Information and related discussion). During this period, cells were imaged using the Incucyte microscopy incubator system to measure cell growth and cell death. The former was tracked by change in confluency and the latter by enumerating CytoTox Green objects (non-viable cells). We observed no significant difference in the increase in cell confluency over 24 h between resting macrophages and those exposed to 50 or 250 µL of AgNP suspension (Fig. 3A,

B, Videos 1, 2 and 3). Similarly, there was no apparent difference in the number of CytoTox Green objects that reflect non-viable cells between the three treatments (Fig. 3A, C, Videos 1, 2, and 3). In comparison, cells treated with staurosporine suffered a decline in confluency and were labelled with CytoTox Green in large numbers (Fig. 3, Video 4). Overall, these data intimate that treatment of cells with a suspension of AgNP was not significantly cytotoxic to RAW macrophages.

AgNP enhance fluorescence of lysosome probes in macrophages

We then proceeded to test if AgNP accumulation in lysosomes could lead to metal-enhanced fluorescence in cells. To account for heterogeneity in uptake, accumulation of dye and AgNP, and possible interference due to proximity of AgNP to each other, we labelled macrophages with two different doses of AgNP: 50 µL or 250 µL of AgNP, as above. Subsequently, cells were allowed to internalize 10 µg/mL BODIPY-cholesterol for 40 min and chased for 10 min to accumulate BODIPY-cholesterol on lysosomes (Hölttä-Vuori et al., 2016). Images were then acquired by spinning disc confocal and analysed for total fluorescence intensity in cells. Importantly, we observed an increase in fluorescence intensity of BODIPY-cholesterol in cells labelled with AgNP, though there was some variability between experiments and cells loaded with different AgNP amounts (Fig. 4A, B). To complement these experiments, we also labelled lysosomes with DQ-BSA, a molecular probe used to measure degradation within lysosomes that yields a green fluorescent BODIPY once the BSA component has been degraded in lysosomes (Marwaha and Sharma, 2017). Again, macrophages were labelled with vehicle or metallic seeds, followed by 10 µg/mL DQ-BSA for 1 h. As with BODIPY-cholesterol, DQ-BSA total fluorescence per cell increased relative to macrophages without AgNP in the lysosomes (Fig. 5A, B). Overall, these data indicate that loading AgNP within lysosomes in macrophages can enhance fluorescence intensity.

AgNP-enhanced fluorescence occurs across the lysosomal bilayer

Our observations suggest that AgNP can enhance fluorescence intensity of molecular probes within lysosomes. We next tested if AgNP could enable metal-enhanced fluorescence of GFP across the lysosomal membrane by expressing LAMP1-GFP, whereby the GFP is located on the cytosolic C-terminal domain of LAMP1 (Falcón-Pérez et al., 2005). Assuming GFP is 10 nm from the plane of the membrane and the lysosomal bilayer, inclusive of the glycocalyx is 30 nm thick, then GFP molecules should be within the effective distance for fluorescence enhancement by AgNP. To test this, we transfected RAW macrophages with plasmids encoding LAMP1-GFP, followed by exposing cells to vehicle, 50 µL or 250 µL AgNP seeds, as before. Cells were imaged and analysed by measuring the total LAMP1-GFP fluorescence using collapsed z-stacks. Notably, we observed a significant increase in the mean total LAMP1-GFP fluorescence in cells that accumulated AgNP relative to vehicle-only (Fig. 6A, B). To determine if metal enhanced fluorescence could also occur in other cell types, we transfected Cos7 cells with plasmid encoding LAMP1-GFP. As with RAW cells, we also observed a boost in LAMP1-GFP fluorescence in Cos7 cells containing AgNP (Fig. 6C, D). Altogether, our observations support the ability of AgNP to enhance fluorescence of GFP across the lysosomal bilayer. This is consistent with the fact that the emission spectrum of GFP, with a maximum at λ_{Em} = 510 nm, is not dissimilar from the fluorescence signature of BODIPY (Fig. 1B) and, thus, suitable to experience MEF by our AgNP.

AgNP-enhanced fluorescence allows robust imaging conditions while protecting normal lysosome dynamics

We previously showed that photo-toxicity during spinning disc confocal imaging can interfere with lysosome dynamics due to ROS accumulation (Choy et al., 2018; Saffi et al., 2021). We hypothesized we could use AgNP-mediated fluorescence enhancement to lower photo-toxicity during imaging of lysosome dynamics in RAW cells. To test this, we labelled cells with DQ-BSA as before and tracked cells at high or low laser power over 5 min at 0.2 frames/s. We then subjected lysosomes to tracking analysis. Consistent with ROS-mediated damage that we observed previously (Choy et al., 2018; Saffi et al., 2021), while high laser power produces images with excellent signal-to-noise ratio, lysosomes became less motile in RAW macrophages (Fig. 7A, E, Video 5). In comparison, cells with low laser power displayed low signal-to-noise ratio and tracking lysosomes was not reliable (Fig. 7A, Video 6). However, cells that internalized 50 µL or 250 µL AgNP but were exposed with low laser power now displayed enhanced DQ-BSA signal-to-noise ratio (Fig. 7A, Videos 7 and 8). Importantly, we could track lysosome dynamics under these conditions, observing that lysosomes were significantly more motile and dynamic than in cells without AgNP particles and exposed to high light energy (Fig. 7B, Videos 5-8). Overall, we propose that AgNP-loading of lysosomes may be a useful tool to enhance fluorescence of lysosome-targeted probes, reducing the need for strong light energy or exposure, dropping photo-toxicity, which ultimately minimizes artifacts during live-cell imaging.

Discussion

Fluorescence microscopy is a critical tool in biological studies and applications. However, it is hampered by the need to use excessive light energy to generate images with good signal-to-noise ratio. This ultimately leads to the generation of reactive oxygen species that can photobleach the fluorescent probes and cause be toxic to living samples. Photobleaching is not only inconvenient,

but can limit observations, while phototoxicity can lead to artifactual observations (Boudreau et al., 2016; Han et al., 2017; Icha et al., 2017; Tinevez et al., 2012; Waldchen et al., 2015). Over the years, improved fluorochromes, camera and photodetector sensitivity, computer algorithms, and elegant design of dyes with suitable physicochemical properties have reduced the light intensity and/or exposure needed to obtain good signal-to-noise (Boutros et al., 2015; Jing et al., 2021; Lidke and Lidke, 2012). Despite these efforts, photobleaching and phototoxicity remain significant problems in live-cell imaging.

MEF holds great promise as a tool to augment spectroscopic and fluorescence-based applications (Bouhelier et al., 2004; Ekgasit et al., 2004b; Hodgson et al., 2020; J. Kneipp et al., 2006; K. Kneipp et al., 2006; Lakowicz et al., 2003; Petryayeva and Krull, 2011). Indeed, plasmonic metal nanoparticles can impact the behaviour of organic chromophores in a number of ways, including enhancing molecular fluorescence. From the perspective of the fluorochrome, this type of enhancement is originated by intensification of the incident electromagnetic field, via plasmonic excitation of the metallic nanostructures. Much of the relevant literature acknowledges the effects of nanoparticle shape, size, orientation, interparticle spacing or nanoparticle-dye separation upon ensemble averaged fluorescence enhancement factors (Anger et al., 2006; Deng et al., 2013; Dragan and Geddes, 2011; Dutta Choudhury et al., 2012; Fort and Grésillon, 2008; Fothergill et al., 2018; Kinoshita et al., 2015; Lakowicz et al., 2008, 2002; Lin and Chen, 2015; Wei et al., 2018; Xie et al., 2013, 2008). However, it is also critical to emphasize the importance of the optical properties of all the different components of the system i.e., fluorophores and nanoparticles working synergistically to achieve MEF. Interestingly, the spectral position of the plasmophore's enhanced emission is nearly indistinguishable from that of fluorescence emission in free space: as such, applications of MEF abound for the magnification of fluorescence for

bioimaging. For example, AgNP can enhance fluorescence of conjugated DNA oligomers (Ekgasit et al., 2004a; Lakowicz et al., 2003) and focal fields mapping (Bouhelier et al., 2004), while enhancement of single-molecule fluorescence by AgNP was exploited for the study of ribosomal mRNA translation (Bharill et al., 2011). Moreover, gold nanoparticles (AuNP) have been used to enhance single-molecule Raman spectroscopic imaging within cells, including within endosomes (J. Kneipp et al., 2006; K. Kneipp et al., 2006). However, to the best of our knowledge, AgNP have not been tested for their ability to enhance fluorescence intracellularly in living cells. Herein, we showed that RAW macrophages fed AgNP by pinocytosis leads to enhanced fluorescence of BODIPY-conjugated lysosome-targeted probes and GFP anchored to the cytoplasmic face of the lysosomal membrane as a LAMP1-GFP chimera. We demonstrate that this enhances signal-to-noise ratio affording a reduction in laser intensity, which abates phototoxicity, ultimately preserving cell function as seen in the preservation of lysosome motility.

Loading of AgNP into the endo-lysosomal system of cells is a promising tool to enhance fluorescence of endo-lysosomal probes, affording one to reduce light intensity and/or exposure. This is particularly important for imaging lysosome dynamics in macrophages, which have proven to be sensitive to photo-damage during spinning disc confocal microscopy and reactive oxygen species (Choy et al., 2018; Saffi et al., 2021). In fact, we have observed that lysosome motility and fusion-fission cycles can be altered during imaging and by reactive oxygen species (Choy et al., 2018; Saffi et al., 2021). Though light-induced alteration to lysosome function may depend on cell type, loading lysosomes with AgNP may be instrumental to visualize lysosome dynamics during confocal microscopy.

It is important to note that the conditions for AgNP-mediated enhancing imaging of lysosomes will need optimization by the user, including consideration on the cell type under study,

and the specific lysosomal probe. Moreover, future work is needed to explore the optimization of nanoparticles with different structure/properties relationships (e.g., size and shape) for which the plasmon resonance will need to be finetuned in order to enhance fluorescence of probes emitting at different wavelengths. Finally, AgNP may have different uses to enhance fluorescence in cells. Here, we used bulk pinocytosis of AgNP by macrophages, expecting AgNP to localize to lysosomes. However, it may be possible to enrich AgNP in endosomes with short pulse-chase periods. Alternatively, conjugating AgNP to ligands known to cycle through the endosomal system such as transferrin may allow for endosomal imaging (Roberts et al., 2006; van Dam and Stoorvogel, 2002). Similarly, AgNP may be conjugated to particulates like bacteria and polysterene beads to track phagosomes and study phagocytosis (Fountain et al., 2021).

Limitations of Study

Using our specific irradiation instruments, power, and ratio of reagents, we obtained highly reproducible AgNP suspension in terms of particle number, size, and shape. However, as these specifics may change between labs and users, initial production of AgNP by other workers will need to be tested and standardized. Moreover, while our study clearly demonstrates that AgNP can enhance "green" fluorochromes within cells, future studies should develop AgNP with distinct spectral properties to determine if MEF can be achieved within cells when using fluorophores with different excitation/emission properties. Lastly, while loading AgNP into RAW macrophages did not impair cell growth or aggravate cell death within 24 h of observation, other aspects of cellular physiology may be impacted by AgNP-loading, which will need to be assessed and controlled for.

Acknowledgements

This work was supported by the Canada Research Chair Program (950-232333) and associated contributions from Ryerson University, Project Grants from the Canadian Institutes of Health Research Project Grant (123373 and PJT-166047), the Canada Foundation for Innovation (32957) and associated contributions from the Ministry of Economic Development, Job Creation and Trade (32957) and Ryerson University to R.J.B. In addition, this work was supported by Discovery Grants from the Natural Sciences and Engineering Research Council to C.N.A. (RGPIN-2016-04371) and S.I. (RGPIN-2018-04161) and the Ryerson University Faculty of Science Dean's Research Fund.

Author Contributions

SAS is main experimental contributor to this work and performed experimental design, data acquisition, interpretation, co-writing, and figure preparation. AS assisted in data acquisition and interpretation, and figure preparation. GKH and MS established foundational data for this research and helped in experimental design. CNA, SI, and RJB were responsible for experimental design, resource acquisition, supervision, co-writing, figure preparation, and editing.

Declaration of interests

Authors declare no conflicts of interest.

References

Anger, P., Bharadwaj, P., Novotny, L., 2006. Enhancement and quenching of single-molecule fluorescence. Phys. Rev. Lett. 96, 113002. doi:10.1103/PhysRevLett.96.113002

Aslan, K., Leonenko, Z., Lakowicz, J.R., Geddes, C.D., 2005. Annealed silver-island films for applications in metal-enhanced fluorescence: Interpretation in terms of radiating plasmons. J. Fluoresc. 15, 643–654. doi:10.1007/s10895-005-2970-z

Balderhaar, H.J.K., Ungermann, C., 2013. CORVET and HOPS tethering complexes - coordinators of endosome and lysosome fusion. J. Cell Sci. 126, 1307–16. doi:10.1242/jcs.107805

Barnes, W.L., Dereux, A., Ebbesen, T.W., 2003. Surface plasmon subwavelength optics. Nature. doi:10.1038/nature01937

Bharill, S., Chen, C., Stevens, B., Kaur, J., Smilansky, Z., Mandecki, W., Gryczynski, I., Gryczynski, Z., Cooperman, B.S., Goldman, Y.E., 2011. Enhancement of single-molecule fluorescence signals by colloidal silver nanoparticles in studies of protein translation. ACS Nano 5, 399–407. doi:10.1021/nn101839t

Bissig, C., Hurbain, I., Raposo, G., van Niel, G., 2017. PIKfyve activity regulates reformation of terminal storage lysosomes from endolysosomes. Traffic 18, 747–757. doi:10.1111/tra.12525

Boudreau, C., Wee, T.L., Duh, Y.R., Couto, M.P., Ardakani, K.H., Brown, C.M., 2016. Excitation light dose engineering to reduce photo-bleaching and photo-toxicity. Sci. Rep. 6, 1–12. doi:10.1038/srep30892

Bouhelier, A., Beversluis, M.R., Novotny, L., 2004. Applications of field-enhanced near-field optical microscopy, in: Ultramicroscopy. Ultramicroscopy, pp. 413–419. doi:10.1016/j.ultramic.2003.10.007

Boutros, M., Heigwer, F., Laufer, C., 2015. Microscopy-Based High-Content Screening. Cell. doi:10.1016/j.cell.2015.11.007

Bright, N.A., Gratian, M.J., Luzio, J.P., 2005. Endocytic delivery to lysosomes mediated by

concurrent fusion and kissing events in living cells. Curr. Biol. 15, 360–365. doi:10.1016/j.cub.2005.01.049

Choy, C.H., Saffi, G., Gray, M.A., Wallace, C., Dayam, R.M., Ou, Z.Y.A., Lenk, G., Puertollano, R., Watkins, S.C., Botelho, R.J., 2018. Lysosome enlargement during inhibition of the lipid kinase PIKfyve proceeds through lysosome coalescence. J. Cell Sci. 131, jcs213587. doi:10.1242/JCS.213587

Deng, W., Xie, F., Baltar, H.T.M.C.M., Goldys, E.M., 2013. Metal-enhanced fluorescence in the life sciences: Here, now and beyond. Phys. Chem. Chem. Phys. doi:10.1039/c3cp50206f

Dogantzis, N.P., Hodgson, G.K., Impellizzeri, S., 2020. Optical writing and single molecule reading of photoactivatable and silver nanoparticle-enhanced fluorescence. Nanoscale Adv. 2, 1956–1966. doi:10.1039/d0na00049c

Dragan, A.I., Geddes, C.D., 2011. Excitation volumetric effects (EVE) in metal-enhanced fluorescence. Phys. Chem. Chem. Phys. 13, 3831–3838. doi:10.1039/c0cp01986k

Dragan, A.I., Mali, B., Geddes, C.D., 2013. Wavelength-dependent metal-enhanced fluorescence using synchronous spectral analysis. Chem. Phys. Lett. 556, 168–172. doi:10.1016/j.cplett.2012.11.035

Dutta Choudhury, S., Badugu, R., Ray, K., Lakowicz, J.R., 2012. Silver-gold nanocomposite substrates for metal-enhanced fluorescence: Ensemble and single-molecule spectroscopic studies. J. Phys. Chem. C 116, 5042–5048. doi:10.1021/jp212242x

Ekgasit, S., Stengel, G., Knoll, W., 2004a. Concentration of dye-labeled nucleotides incorporated into DNA determined by surface plasmon resonance-surface plasmon fluorescence spectroscopy. Anal. Chem. 76, 4747–4755. doi:10.1021/ac0495586

Ekgasit, S., Thammacharoen, C., Yu, F., Knoll, W., 2004b. Evanescent Field in Surface Plasmon

Resonance and Surface Plasmon Field-Enhanced Fluorescence Spectroscopies. Anal. Chem. 76, 2210–2219. doi:10.1021/ac035326f

Falcón-Pérez, J.M., Nazarian, R., Sabatti, C., Dell'Angelica, E.C., 2005. Distribution and dynamics of Lamp1-containing endocytic organelles in fibroblasts deficient in BLOC-3. J. Cell Sci. 118, 5243–5255. doi:10.1242/jcs.02633

Fort, E., Grésillon, S., 2008. Surface enhanced fluorescence. J. Phys. D. Appl. Phys. 41, 013001. doi:10.1088/0022-3727/41/1/013001

Fothergill, S.M., Joyce, C., Xie, F., 2018. Metal enhanced fluorescence biosensing: From ultra-violet towards second near-infrared window. Nanoscale 10, 20914–20929. doi:10.1039/c8nr06156d

Fountain, A., Inpanathan, S., Alves, P., Verdawala, M.B., Botelho, R.J., 2021. Phagosome maturation in macrophages: Eat, digest, adapt, and repeat. Adv. Biol. Regul. doi:10.1016/j.jbior.2021.100832

Fu, Y., Lakowicz, J.R., 2007. Single-molecule studies of enhanced fluorescence on silver island films. Plasmonics 2, 1–4. doi:10.1007/s11468-007-9023-1

Fu, Y., Zhang, J., Lakowicz, J.R., 2007. Plasmonic enhancement of single-molecule fluorescence near a silver nanoparticle. J. Fluoresc. 17, 811–816. doi:10.1007/s10895-007-0259-0

Golian, K.P., Akari, A.S., Hodgson, G.K., Impellizzeri, S., 2021. Fluorescence activation, patterning and enhancement with photogenerated radicals, a prefluorescent probe and silver nanostructures. RSC Adv. 11, 5163–5171. doi:10.1039/d0ra09565f

Han, Y., Li, M., Qiu, F., Zhang, M., Zhang, Y.H., 2017. Cell-permeable organic fluorescent probes for live-cell long-term super-resolution imaging reveal lysosome-mitochondrion interactions. Nat. Commun. 8. doi:10.1038/s41467-017-01503-6

Hao, E., Schatz, G.C., 2004. Electromagnetic fields around silver nanoparticles and dimers. J. Chem. Phys. 120, 357–366. doi:10.1063/1.1629280

Hodgson, G.K., Dogantzis, N.P., Impellizzeri, S., 2020. Single molecule techniques can distinguish the photophysical processes governing metal-enhanced fluorescence. J. Phys. Chem. C 124, 28298–28305. doi:10.1021/acs.jpcc.0c09157

Hölttä-Vuori, M., Sezgin, E., Eggeling, C., Ikonen, E., 2016. Use of BODIPY-Cholesterol (TF-Chol) for Visualizing Lysosomal Cholesterol Accumulation. Traffic 17, 1054–1057. doi:10.1111/tra.12414

Hong, N.H., Qi, A., Weaver, A.M., 2015. PI(3,5)P2 controls endosomal branched actin dynamics by regulating cortactin-Actin interactions. J. Cell Biol. 210, 753–769. doi:10.1083/jcb.201412127

Huotari, J., Helenius, A., 2011. Endosome maturation. EMBO J. 30, 3481–3500. doi:10.1038/emboj.2011.286

Icha, J., Weber, M., Waters, J.C., Norden, C., 2017. Phototoxicity in live fluorescence microscopy, and how to avoid it. BioEssays 39, 1700003. doi:10.1002/bies.201700003

Inpanathan, S., Botelho, R.J., 2019. The Lysosome Signaling Platform: Adapting With the Times. Front. Cell Dev. Biol. 7, 113. doi:10.3389/fcell.2019.00113

Jensen, E.C., 2013. Overview of Live-Cell Imaging: Requirements and Methods Used. Anat. Rec. 296, 1–8. doi:10.1002/ar.22554

Jing, Y., Zhang, C., Yu, B., Lin, D., Qu, J., 2021. Super-Resolution Microscopy: Shedding New Light on In Vivo Imaging. Front. Chem. doi:10.3389/fchem.2021.746900

Johansson, M., Rocha, N., Zwart, W., Jordens, I., Janssen, L., Kuijl, C., Olkkonen, V.M., Neefjes, J., 2007. Activation of endosomal dynein motors by stepwise assembly of Rab7-RILP-

p150Glued, ORP1L, and the receptor βIII spectrin. J. Cell Biol. 176, 459–471. doi:10.1083/jcb.200606077

Keren-Kaplan, T., Sarić, A., Ghosh, S., Williamson, C.D., Jia, R., Li, Y., Bonifacino, J.S., 2022. RUFY3 and RUFY4 are ARL8 effectors that promote coupling of endolysosomes to dynein-dynactin. Nat. Commun. 13, 1506. doi:10.1038/s41467-022-28952-y

Kinoshita, T., Nguyen, D.Q., Nishino, T., Nakao, H., Shiigi, H., Nagaoka, T., 2015. Fluorescence enhancement of nanoraspberry hot-spot source composed of gold nanoparticles and aniline oligomers. Anal. Sci. 31, 487–493. doi:10.2116/analsci.31.487

Kiselyov, K.K., Ahuja, M., Rybalchenko, V., Patel, S., Muallem, S.,. The intracellular Ca^{2+} channels of membrane traffic. Channels (Austin). 6, 344–51. doi:10.4161/chan.21723

Kneipp, J., Kneipp, H., McLaughlin, M., Brown, D., Kneipp, K., 2006. In vivo molecular probing of cellular compartments with gold nanoparticles and nanoaggregates. Nano Lett. 6, 2225–2231. doi:10.1021/nl061517x

Kneipp, K., Kneipp, H., Kneipp, J., 2006. Surface-enhanced raman scattering in local optical fields of silver and gold nanoaggregates - From single-molecule raman spectroscopy to ultrasensitive probing in live cells. Acc. Chem. Res. 39, 443–450. doi:10.1021/ar050107x

Knoblauch, R., Ben Hamo, H., Marks, R., Geddes, C.D., 2020. Spectral Distortions in Metal-Enhanced Fluorescence: Experimental Evidence for Ultra-Fast and Slow Transitions. J. Phys. Chem. C 124, 4723–4737. doi:10.1021/acs.jpcc.9b11055

Kumar, G., Chawla, P., Dhiman, N., Chadha, S., Sharma, S., Sethi, K., Sharma, M., Tuli, A., 2022. RUFY3 links Arl8b and JIP4-Dynein complex to regulate lysosome size and positioning. Nat. Commun. 13, 1540. doi:10.1038/s41467-022-29077-y

Lakowicz, J.R., 2005. Radiative decay engineering 5: Metal-enhanced fluorescence and plasmon

emission. Anal. Biochem. 337, 171–194. doi:10.1016/j.ab.2004.11.026

Lakowicz, J.R., Malicka, J., Gryczynski, I., 2003. Silver particles enhance emission of fluorescent DNA oligomers. Biotechniques 34, 62–68. doi:10.2144/03341st01

Lakowicz, J.R., Ray, K., Chowdhury, M., Szmacinski, H., Fu, Y., Zhang, J., Nowaczyk, K., 2008. Plasmon-controlled fluorescence: A new paradigm in fluorescence spectroscopy. Analyst. doi:10.1039/b802918k

Lakowicz, J.R., Shen, Y., D'Auria, S., Malicka, J., Fang, J., Gryczynski, Z., Gryczynski, I., 2002. Radiative decay engineering: 2. Effects of silver island films on fluorescence intensity, lifetimes, and resonance energy transfer. Anal. Biochem. 301, 261–277. doi:10.1006/abio.2001.5503

Lidke, D.S., Lidke, K.A., 2012. Advances in high-resolution imaging - techniques for three-dimensional imaging of cellular structures. J. Cell Sci. 125, 2571–2580. doi:10.1242/jcs.090027

Lin, H.H., Chen, I.C., 2015. Study of the Interaction between Gold Nanoparticles and Rose Bengal Fluorophores with Silica Spacers by Time-Resolved Fluorescence Spectroscopy. J. Phys. Chem. C 119, 26663–26671. doi:10.1021/acs.jpcc.5b08477

Liz-Marzán, L.M., 2006. Tailoring surface plasmons through the morphology and assembly of metal nanoparticles. Langmuir 22, 32–41. doi:10.1021/la0513353

Luzio, J.P., Pryor, P.R., Bright, N.A., 2007. Lysosomes: Fusion and function. Nat. Rev. Mol. Cell Biol. doi:10.1038/nrm2217

Malicka, J., Gryczynski, I., Fang, J., Lakowicz, J.R., 2003. Fluorescence spectral properties of cyanine dye-labeled DNA oligomers on surfaces coated with silver particles. Anal. Biochem. 317, 136–146. doi:10.1016/S0003-2697(03)00005-8

Marwaha, R., Sharma, M., 2017. DQ-Red BSA Trafficking Assay in Cultured Cells to Assess Cargo Delivery to Lysosomes. BIO-PROTOCOL 7. doi:10.21769/bioprotoc.2571

Moen, E., Bannon, D., Kudo, T., Graf, W., Covert, M., Van Valen, D., 2019. Deep learning for cellular image analysis. Nat. Methods. doi:10.1038/s41592-019-0403-1

Moores, A., Goettmann, F., 2006. The plasmon band in noble metal nanoparticles: An introduction to theory and applications. New J. Chem. doi:10.1039/b604038c

Naslavsky, N., Caplan, S., 2018. The enigmatic endosome - Sorting the ins and outs of endocytic trafficking. J. Cell Sci. doi:10.1242/jcs.216499

Norris, A., Grant, B.D., 2020. Endosomal microdomains: Formation and function. Curr. Opin. Cell Biol. doi:10.1016/j.ceb.2020.02.018

Odom, T.W., Schatz, G.C., 2011. Introduction to plasmonics. Chem. Rev. doi:10.1021/cr2001349

Ouyang, W., Aristov, A., Lelek, M., Hao, X., Zimmer, C., 2018. Deep learning massively accelerates super-resolution localization microscopy. Nat. Biotechnol. 36, 460–468. doi:10.1038/nbt.4106

Peterson, A.W., Halter, M., Plant, A.L., Elliott, J.T., 2016. Surface plasmon resonance microscopy: Achieving a quantitative optical response. Rev. Sci. Instrum. 87. doi:10.1063/1.4962034

Petryayeva, E., Krull, U.J., 2011. Localized surface plasmon resonance: Nanostructures, bioassays and biosensing-A review. Anal. Chim. Acta. doi:10.1016/j.aca.2011.08.020

Pierzyńska-Mach, A., Janowski, P.A., Dobrucki, J.W., 2014. Evaluation of acridine orange, LysoTracker Red, and quinacrine as fluorescent probes for long-term tracking of acidic vesicles. Cytom. Part A 85, 729–737. doi:10.1002/cyto.a.22495

Roberts, E.A., Chua, J., Kyei, G.B., Deretic, V., 2006. Higher order Rab programming in

phagolysosome biogenesis. J. Cell Biol. 174, 923–929. doi:10.1083/jcb.200603026

Rust, M.J., Bates, M., Zhuang, X., 2006. Sub-diffraction-limit imaging by stochastic optical reconstruction microscopy (STORM). Nat. Methods 3, 793–795. doi:10.1038/nmeth929

Saffi, G.T., Botelho, R.J., 2019. Lysosome Fission: Planning for an Exit. Trends Cell Biol. doi:10.1016/j.tcb.2019.05.003

Saffi, G.T., Tang, E., Mamand, S., Inpanathan, S., Fountain, A., Salmena, L., Botelho, R.J., 2021. Reactive oxygen species prevent lysosome coalescence during PIKfyve inhibition. PLoS One 16. doi:10.1371/journal.pone.0259313

Shashkova, S., Leake, M.C., 2017. Single-molecule fluorescence microscopy review: Shedding new light on old problems. Biosci. Rep. doi:10.1042/BSR20170031

Shtengel, G., Galbraith, J.A., Galbraith, C.G., Lippincott-Schwartz, J., Gillette, J.M., Manley, S., Sougrat, R., Waterman, C.M., Kanchanawong, P., Davidson, M.W., Fetter, R.D., Hess, H.F., 2009. Interferometric fluorescent super-resolution microscopy resolves 3D cellular ultrastructure. Proc. Natl. Acad. Sci. U. S. A. 106, 3125–3130. doi:10.1073/pnas.0813131106

Stamplecoskie, K.G., Scaiano, J.C., 2012. Silver as an example of the applications of photochemistry to the synthesis and uses of nanomaterials, in: Photochemistry and Photobiology. John Wiley & Sons, Ltd, pp. 762–768. doi:10.1111/j.1751-1097.2012.01103.x

Stamplecoskie, K.G., Scaiano, J.C., 2010. Light emitting diode irradiation can control the morphology and optical properties of silver nanoparticles. J. Am. Chem. Soc. 132, 1825–1827. doi:10.1021/ja910010b

Tinevez, J.Y., Dragavon, J., Baba-Aissa, L., Roux, P., Perret, E., Canivet, A., Galy, V., Shorte, S., 2012. A quantitative method for measuring phototoxicity of a live cell imaging microscope, in: Methods in Enzymology. Academic Press Inc., pp. 291–309. doi:10.1016/B978-0-12-

391856-7.00039-1

Tinevez, J.Y., Perry, N., Schindelin, J., Hoopes, G.M., Reynolds, G.D., Laplantine, E., Bednarek, S.Y., Shorte, S.L., Eliceiri, K.W., 2017. TrackMate: An open and extensible platform for single-particle tracking. Methods 115, 80–90. doi:10.1016/j.ymeth.2016.09.016

van Dam, E.M., Stoorvogel, W., 2002. Dynamin-dependent transferrin receptor recycling by endosome-derived clathrin-coated vesicles. Mol. Biol. Cell 13, 169–82. doi:10.1091/mbc.01-07-0380

Waldchen, S., Lehmann, J., Klein, T., Van De Linde, S., Sauer, M., 2015. Light-induced cell damage in live-cell super-resolution microscopy. Sci. Rep. 5. doi:10.1038/srep15348

Wei, L.Y., Huang, K.S., Lin, H.H., Wu, Y.P., Tan, K.T., Lee, Y.Y., Chen, I.C., 2018. Kinetic Mechanism of Metal Enhanced Fluorescence by Gold Nanoparticle with Avidin-Biotin as Spacer and by Gold-Silver Core-Shell Nanoparticle Using Fluorescence Lifetime Image Microscopy. J. Phys. Chem. C 122, 28431–28438. doi:10.1021/acs.jpcc.8b10440

Xie, F., Baker, M.S., Goldys, E.M., 2008. Enhanced fluorescence detection on homogeneous gold colloid self-assembled monolayer substrates. Chem. Mater. 20, 1788–1797. doi:10.1021/cm703121m

Xie, F., Centeno, A., Ryan, M.R., Riley, D.J., Alford, N.M., 2013. Au nanostructures by colloidal lithography: From quenching to extensive fluorescence enhancement. J. Mater. Chem. B 1, 536–543. doi:10.1039/c2tb00278g

Figure legends

Figure 1: Synthesis and spectral properties of AgNP and BODIPY. A. Schematic of the synthesis pathway for AgNP seeds. **B.** Normalized steady-state absorption (20 °C, CH_3CN) and emission spectra of $BODIPY^{493/503}$ (20 °C, CH_3CN, λ_{Ex} = 460 nm), and extinction spectrum of AgNP (20 °C, water).

Figure 2: AgNP enhances fluorescence intensity of BODIPY embedded in a gelatin matrix. A, C. A mixture of gelatin and BODIPY (A) or of gelatin and BODIPY-cholesterol (C) was casted on top of coverslips with no AgNP or with a AgNP-film dried onto the coverslip. Gelatin films were then imaged by spinning disc confocal microscopy. Images are shown as false-colour, where white-yellow is highest intensity and black-blue is lowest intensity. Scale bar = 10 µm. **B, D.** The mean fluorescence intensity of images was quantified including images with AgNP dried but no fluorochome added (first column). The means ± SEM from N=5 experiments are shown. The mean was normalized to the fluorochome-only condition. One-way ANOVA and Tukey's post-hoc test were used to compare means, * $p<0.05$.

Figure 3: AgNP do not cause cytotoxicity in macrophages. **A.** RAW macrophages were kept resting, or they were treated over 24 h with 50 µL AgNP, 250 µL AgNP, or 5 µM staurosporine, while imaging in an Incucyte Incubator System. Confluency was tracked as an indicator of cell growth, while then number of CellTox Green particulates indicated cell death. Still frames at the

indicated time points and treatments are shown. Scale bar = 400 µm. Images correspond to Supplemental Videos 1 through 4. **B.** Percent confluency over 24 h normalized to resting cells. **C.** CellTox Green particles normalized to respective confluency for each condition shown. For B and C, shown are the mean ± SEM of N=4.

Figure 4: AgNP-enhanced fluorescence of BODIPY-cholesterol in RAW macrophages. **A.** RAW cells were fed vehicle, 50 µL AgNP, or 250 µL AgNP, followed by 10 µg/mL BODIPY-cholesterol for 40 min and chased for 10 min. Cells were then imaged by spinning disc confocal microscopy. Images are shown in grayscale (top) or false-colour (bottom), where white-yellow is highest intensity and black-blue is lowest intensity. Scale bar = 10 µm. **B.** Quantification of fluorescence intensity of BODIPY-cholesterol per cell, normalized to cells without AgNP. Shown is the mean ± SEM from N=4 experiments, where 15-30 cells were quantified per condition per experiment. One-way ANOVA and Tukey's post-hoc test were used to compare means, * $p<0.05$.

Figure 5: AgNP-enhanced fluorescence of DQ-BSA in RAW macrophages. A. RAW cells were fed vehicle, 50 µL AgNP, or 250 µL AgNP, followed by 10 µg/mL DQ-BSA for 1 h. Cells were then imaged by spinning disc confocal microscopy. Images are shown in grayscale (top) or false-colour (bottom), where white-yellow is highest intensity and black-blue is lowest intensity. Scale bar = 10 µm**. B.** Quantification of fluorescence intensity of DQ-BSA per cell, normalized to cells without AgNP. Shown is the mean ± SEM from N=4 experiments, where 15-30 cells were quantified per condition per experiment. One-way ANOVA and Tukey's post-hoc test were used to compare means, * $p<0.05$.

Figure 6: AgNP boosts fluorescence of LAMP1-GFP. A, C. RAW cells (A) and Cos7 cells (C) were transfected with plasmid encoding LAMP1-GFP. After 24 h, cells were loaded with vehicle, 50 µL AgNP, or 250 µL AgNP. Live-cells were then imaged by spinning disc confocal microscopy and are shown as grayscale (top row) or false-colour (bottom row) as before. Scale bar = 10 µm. **B, D**. The fluorescence intensity of LAMP1-GFP in RAW cells (B) or Cos7 cells (D) was quantified and normalized to control cells with no AgNP. Shown is the mean ± SEM from N=5 independent experiments, where 40-50 cells per condition per experiment were quantified. Means were then tested by one-way ANOVA, followed by Tukey's post-hoc test, where * is $p<0.05$.

Figure 7: AgNP-enhanced fluorescence helps preserve lysosome motility during microscopy imaging. A. RAW cells were loaded with vehicle (top two rows) or AgNP (bottom rows) as before, followed by labelling with DQ-BSA. Cells were then imaged for 5 min at 0.2 frames/second at 10 mW (low) or 50 mW (high) laser power. Individual frames are shown at indicated times and correspond to Videos 5 through 8. Scale bar = 10 µm. Green arrows track individual lysosomes over time. **B.** Time sequences were subjected to particle tracking analysis to measure relative lysosome velocity using TrackMate. Velocity was normalized to control cells with no AgNP and high laser power. Shown is the mean velocity ± SEM from N=3 independent experiments, each with 5 cells per condition per experiment, or total of 15 cells. Means were tested by one-way ANOVA and Tukey's post-hoc test. * indicates $p<0.05$.

Supplemental Video 1: Cell proliferation and death in resting conditions. RAW cells in media containing CellTox Green to detect cell death. No AgNP were added in this condition. Cells were

then imaged every 30 min over 24 h using a 10x objective in the phase channel to track confluency and green channel to track cell death.

Supplemental Video 2: Cell proliferation and death in the presence of 50 µL AgNP. RAW cells in media containing CellTox Green to detect cell death. Cells were exposed to 50 µL of AgNP. Cells were then imaged every 30 min over 24 h using a 10x objective in the phase channel to track confluency and green channel to track cell death.

Supplemental Video 3: Cell proliferation and death in the presence of 250 µL AgNP. RAW cells in media containing CellTox Green to detect cell death and 250 µL of AgNP. Cells were then imaged every 30 min over 24 h using a 10x objective in the phase channel to track confluency and green channel to track cell death.

Supplemental Video 4: Cell proliferation and death in the presence of staurosporine. RAW cells in media containing CellTox Green to detect cell death and 5 µM staurosporine as a positive control for cell death. Cells were imaged every 30 min over 24 h using a 10x objective in the phase channel to track confluency and green channel to track cell death.

Supplemental Video 5: Lysosome dynamics in RAW cells exposed to high laser power. Cells without AgNP were labelled with DQ-BSA for 1 h. Cells were then imaged using 63x objective at 0.2 frames/second for 5 min using 50 mW laser power. Images had strong signal-to-noise ratio but lysosomes became less motile.

Supplemental Video 6: Lysosome dynamics in RAW cells exposed to low laser power and without AgNP. Cells without AgNP were labelled with DQ-BSA for 1 h. Cells were then imaged using 63x objective at 0.2 frames/second for 5 min using 10 mW laser power. Images had poor signal to noise ratio and lysosomes were difficult to track.

Supplemental Video 7: Lysosome dynamics in RAW cells exposed to low laser power and 50 µL of AgNP. Cells were loaded with 50 µL AgNP and labelled with DQ-BSA for 1 h. Cells were then imaged using 63x objective at 0.2 frames/second for 5 min using 10 mW laser power. Images had improved signal to noise ratio and lysosomes retained their dynamic behaviour.

Supplemental Video 8: Lysosome dynamics in RAW cells exposed to low laser power and 250 µL of AgNP. Cells were loaded with 250 µL AgNP and labelled with DQ-BSA for 1 h. Cells were then imaged using 63x objective at 0.2 frames/second for 5 min using 10 mW laser power. Images had improved signal to noise ratio and lysosomes retained their dynamic behaviour.

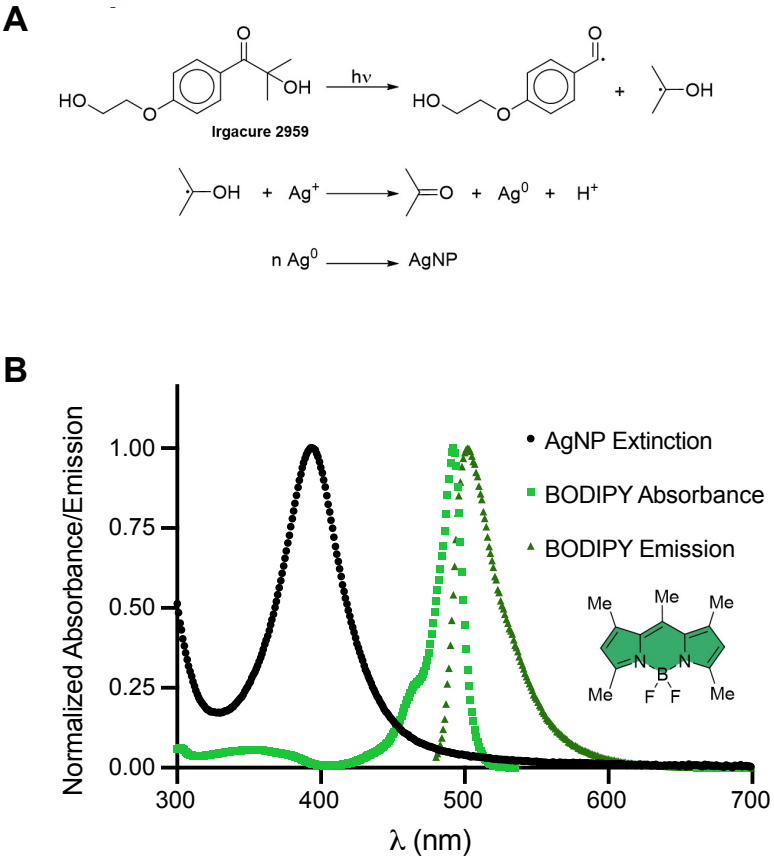
A
HO
O
OH
Irgacure 2959
hν
HO
O
O
+
OH
OH
+ Ag+
O
+ Ag0
+ H+
n Ag0
AgNP
B
Normalized Absorbance/Emission
1.00
0.75
0.50
0.25
0.00
300
400
500
600
700
λ (nm)
AgNP Extinction
BODIPY Absorbance
BODIPY Emission
Me
Me
Me
N
B
N
Me
F
F
Me

Figure 1

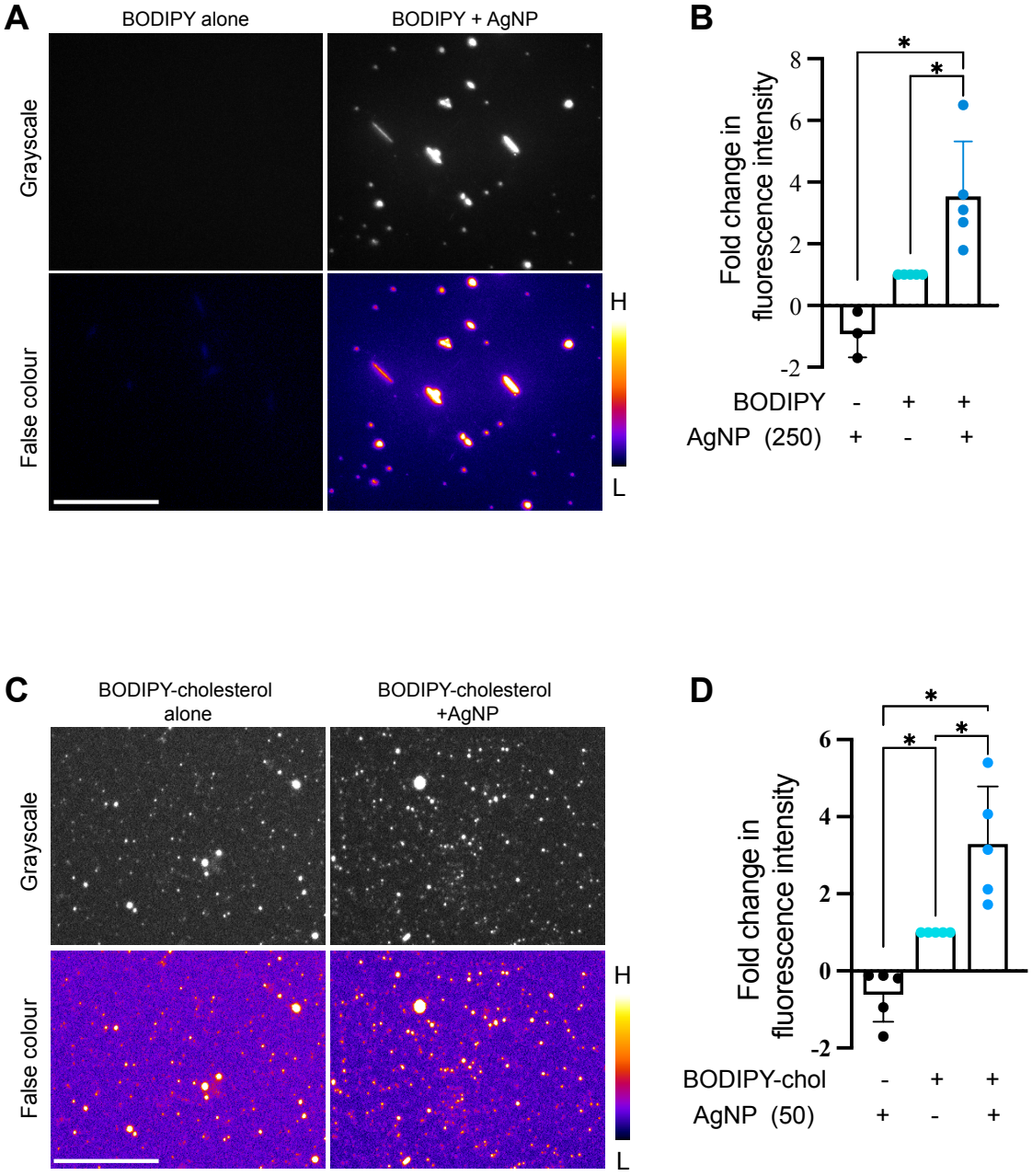
A
BODIPY alone
BODIPY + AgNP
Grayscale
False colour
H
L
B
Fold change in fluorescence intensity
8
6
4
2
0
-2
*
*
BODIPY - + +
AgNP (250) + - +
C
BODIPY-cholesterol alone
BODIPY-cholesterol +AgNP
Grayscale
False colour
H
L
D
Fold change in fluorescence intensity
6
4
2
0
-2
*
*
*
BODIPY-chol - + +
AgNP (50) + - +

Figure 2

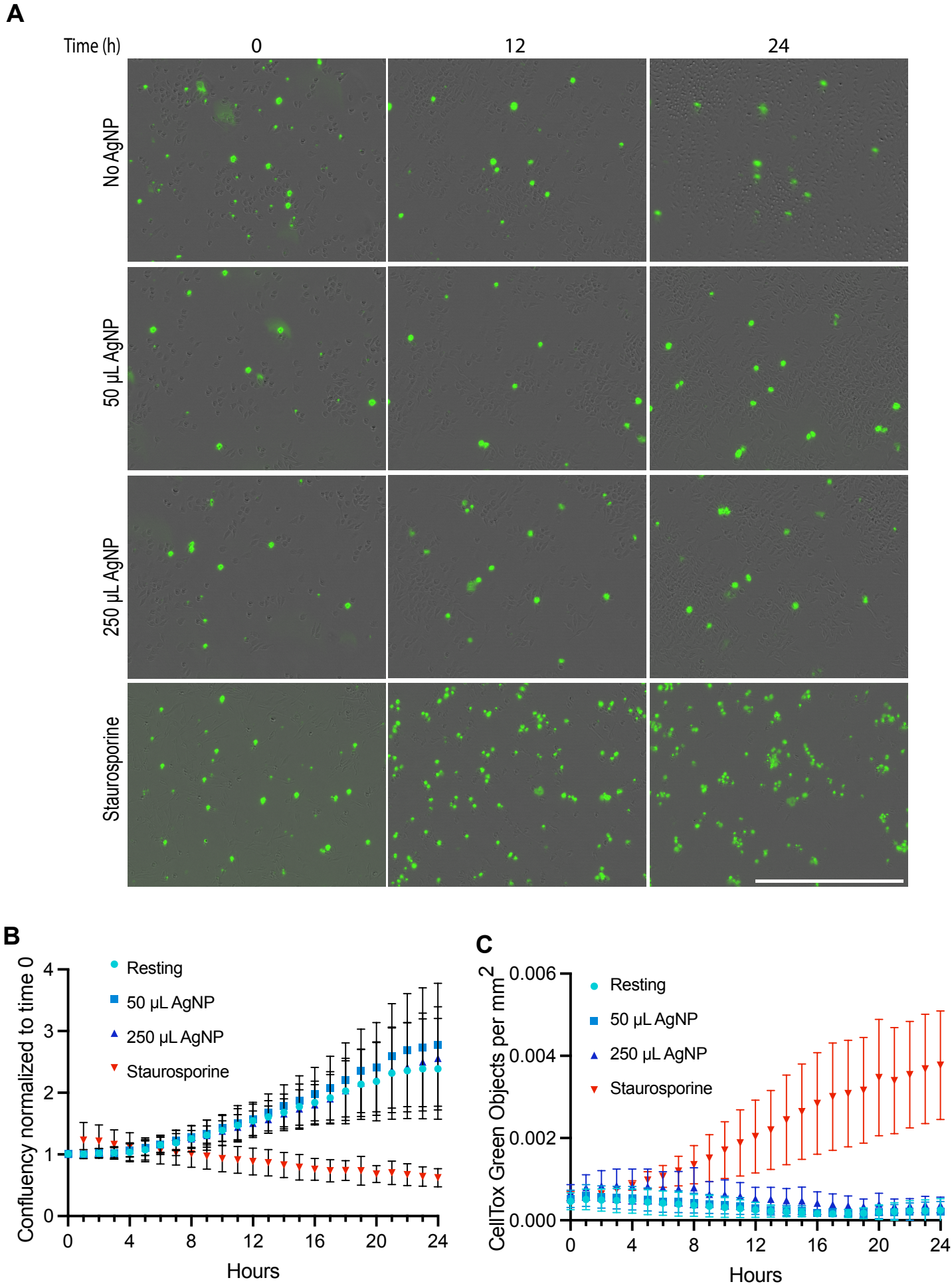
A
Time (h)
0
12
24
No AgNP
50 µL AgNP
250 µL AgNP
Staurosporine
B
Confluency normalized to time 0
Resting
50 µL AgNP
250 µL AgNP
Staurosporine
Hours
C
CellTox Green Objects per mm2
Resting
50 µL AgNP
250 µL AgNP
Staurosporine
Hours

Figure 3

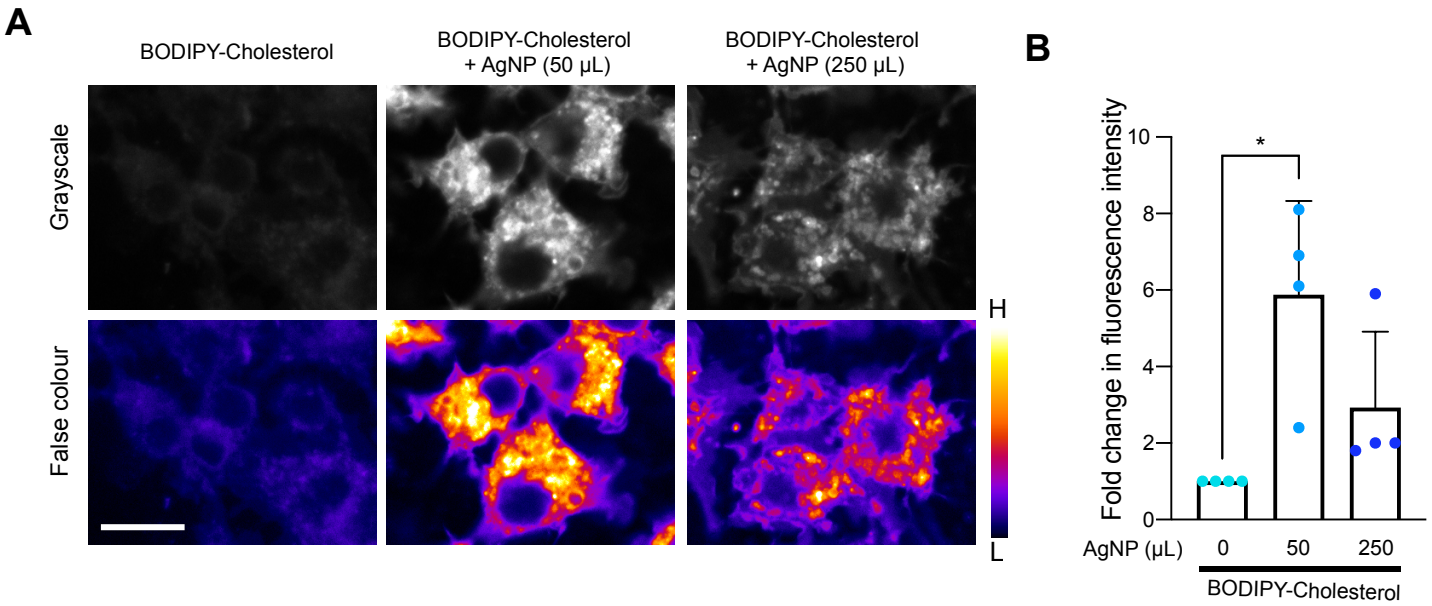
A
BODIPY-Cholesterol
BODIPY-Cholesterol
+ AgNP (50 µL)
BODIPY-Cholesterol
+ AgNP (250 µL)
Grayscale
False colour
H
L
B
Fold change in fluorescence intensity
10
8
6
4
2
0
*
AgNP (µL)
0
50
250
BODIPY-Cholesterol

Figure 4

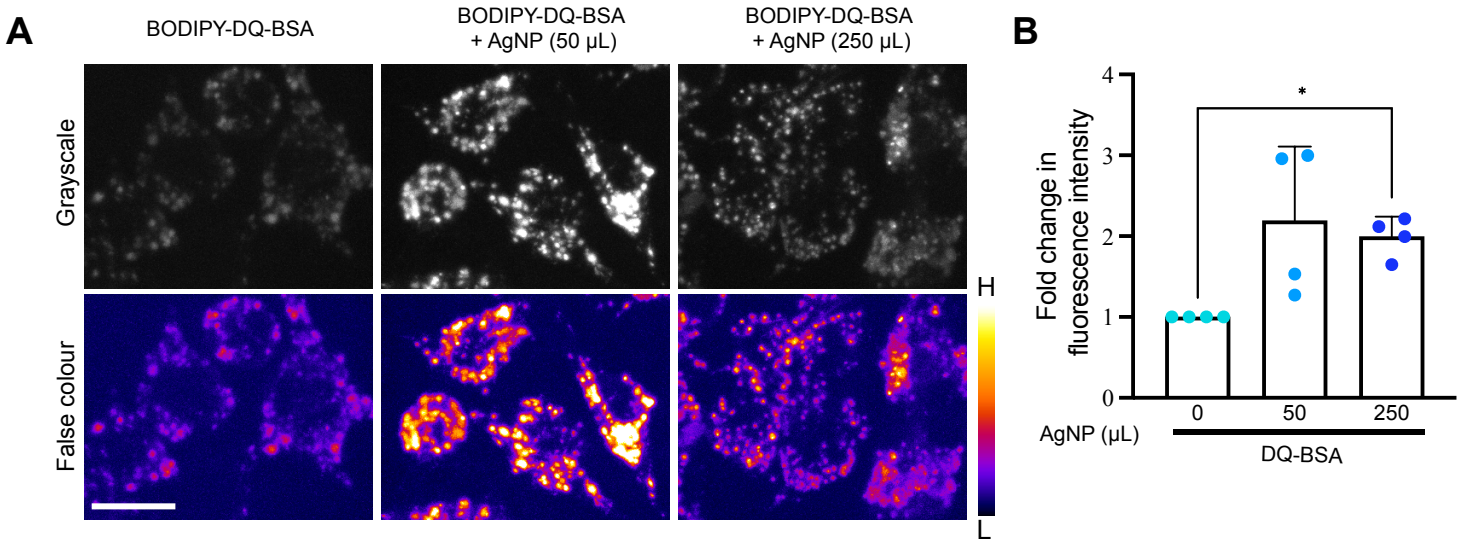
A
BODIPY-DQ-BSA
BODIPY-DQ-BSA
+ AgNP (50 µL)
BODIPY-DQ-BSA
+ AgNP (250 µL)
Grayscale
False colour
H
L
B
Fold change in
fluorescence intensity
4
3
2
1
0
*
0
50
250
AgNP (µL)
DQ-BSA

Figure 5

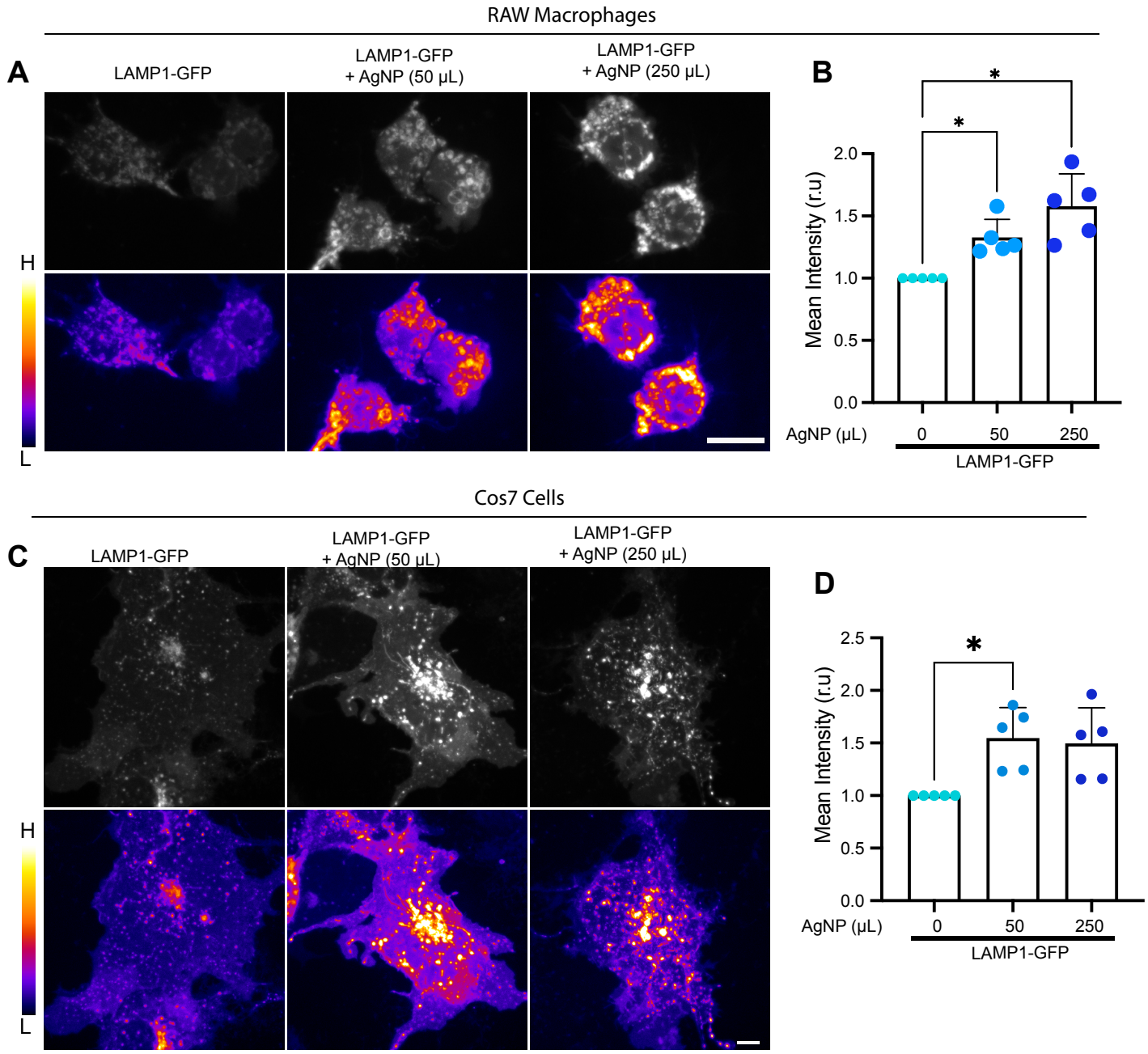
RAW Macrophages
A
LAMP1-GFP
LAMP1-GFP
+ AgNP (50 µL)
LAMP1-GFP
+ AgNP (250 µL)
H
L
B
Mean Intensity (r.u)
2.0
1.5
1.0
0.5
0.0
AgNP (µL)
0
50
250
LAMP1-GFP
Cos7 Cells
C
LAMP1-GFP
LAMP1-GFP
+ AgNP (50 µL)
LAMP1-GFP
+ AgNP (250 µL)
H
L
D
Mean Intensity (r.u)
2.5
2.0
1.5
1.0
0.5
0.0
AgNP (µL)
0
50
250
LAMP1-GFP

Figure 6

A

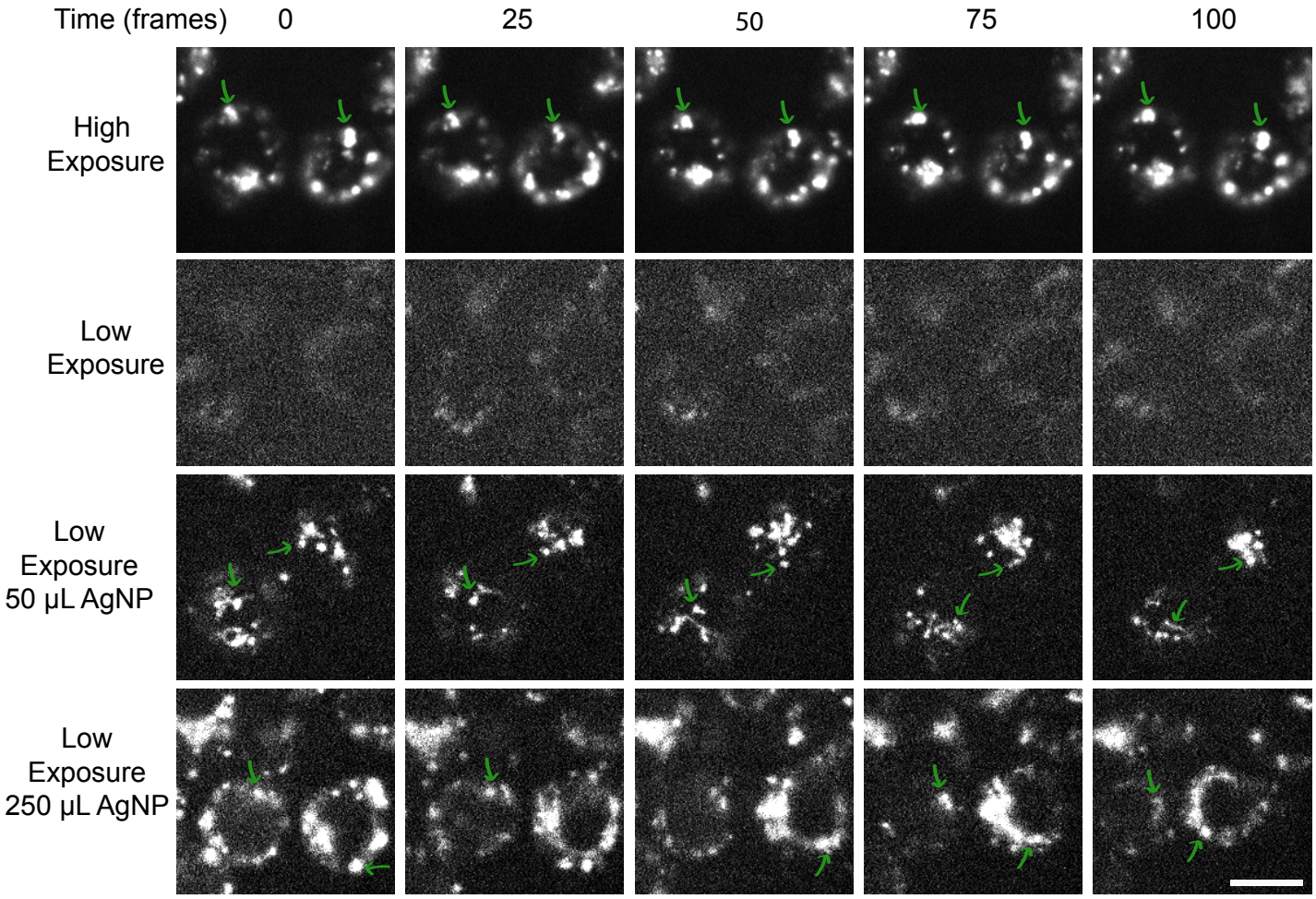
Time (frames)
0
25
50
75
100
High Exposure
Low Exposure
Low Exposure 50 µL AgNP
Low Exposure 250 µL AgNP

B

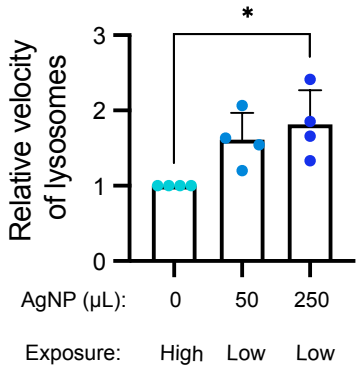
*
Relative velocity of lysosomes
3
2
1
0
AgNP (µL):
0
50
250
Exposure:
High
Low
Low

Figure 7